Published in final edited form as:
NMR Biomed. 2013 October ; 26(10): 1242–1250. doi:10.1002/nbm.2943.

A comparative study of short- and long-TE ^{1}H-MRS at 3T for *in-vivo* detection of 2-hydroxyglutarate in brain tumors

Changho Choi[1,2,3,*], **Sandeep Ganji**[1,2], **Keith Hulsey**[1], **Akshay Madan**[1], **Zoltan Kovacs**[1], **Ivan Dimitrov**[1,4], **Song Zhang**[5], **Kumar Pichumani**[1], **Dianne Mendelsohn**[2], **Bruce Mickey**[3,6,7], **Craig Malloy**[1,2,8,9], **Robert Bachoo**[3,6,8,10], **Ralph DeBerardinis**[11,12], and **Elizabeth Maher**[3,6,8,10]

[1]Advanced Imaging Research Center, University of Texas Southwestern Medical Center, Dallas, Texas, USA

[2]Department of Radiology, University of Texas Southwestern Medical Center, Dallas, Texas, USA

[3]Harold C. Simmons Cancer Center, University of Texas Southwestern Medical Center, Dallas, Texas, USA

[4]Philips Medical Systems, Cleveland, Ohio, USA

[5]Department of Clinical Sciences, University of Texas Southwestern Medical Center, Dallas, Texas, USA

[6]Annette Strauss Center for Neuro-Oncology, University of Texas Southwestern Medical Center, Dallas, Texas, USA

[7]Department of Neurological Surgery, University of Texas Southwestern Medical Center, Dallas, Texas, USA

[8]Department of Internal Medicine, University of Texas Southwestern Medical Center, Dallas, Texas, USA

[9]Veterans Affairs North Texas Health Care System, Dallas, Texas, USA

[10]Department of Neurology and Neurotherapeutics, University of Texas Southwestern Medical Center, Dallas, Texas, USA

[11]Children's Medical Center Research Institute, University of Texas Southwestern Medical Center, Dallas, Texas, USA

[12]McDermott Center for Human Growth and Development, University of Texas Southwestern Medical Center, Dallas, Texas, USA

Abstract

2-hydroxyglutarate (2HG) is produced in gliomas with mutations of isocitrate dehydrogenases (IDH) 1 and 2. The ^{1}H resonances of the J-coupled spins of 2HG are extensively overlapped with signals from other metabolites. Here we report a comparative study at 3T of the utility of the PRESS (point-resolved spectroscopy) sequence with a standard short TE (35 ms) and a long TE (97 ms) which had been theoretically designed for detecting the 2HG 2.25 ppm resonance. The performance of the methods is evaluated using data from phantoms, 7 healthy volunteers, and 22 subjects with IDH-mutated gliomas. The results indicate that TE = 97 ms provides higher detectability of 2HG than TE = 35 ms, and that this improved capability is gained when data are

*Correspondence to: Changho Choi, PhD, Phone: 214-645-2805, FAX: 214-645-2885, changho.choi@utsw.edu.

analyzed with basis spectra that include the effects of the volume localizing radio-frequency and gradient pulses.

Keywords

2-Hydroxyglutarate (2HG); ^{1}H MRS; 3T; Point-resolved spectroscopy (PRESS); Short/Long TE; Volume-localized simulations; Human brain; IDH-mutated gliomas

INTRODUCTION

Mutations in isocitrate dehydrogenase (IDH) 1 and 2 in the majority of World Health Organization grade II and III gliomas and secondary glioblastomas are associated with longer overall survival when compared, grade for grade, with IDH wild type tumors (1,2). IDH1 and IDH2 catalyze the $NADP^{+}$ dependent conversion of isocitrate to α-ketoglutarate in the cytosol and mitochondria, respectively. Somatically-acquired, heterozygous mutations in these enzymes induce a neomorphic enzyme activity, resulting in the production of 2-hydroxyglutarate (2HG) (3–5). As a result, 2HG, normally present only in minute quantities, is increased by orders of magnitude in gliomas bearing IDH mutations. Recent evidence suggests that 2HG may directly contribute to cellular malignancy through epigenetic reprogramming and suppression of cellular differentiation (6). Precise *in vivo* detection of this oncometabolite by MRS may provide a noninvasive diagnostic and prognostic tool for improving the clinical management in patients with IDH-mutated gliomas.

The 2HG molecule contains five non-exchangeable protons from ^{2}CH, $^{3}CH_2$ and $^{4}CH_2$ groups, with resonances at 4.02, 1.83, 1.98, 2.22, and 2.27 ppm at neutral pH (7). The spins are J coupled, giving rise to multiplets at approximately three locations at 3T; 4.02, 1.9, and 2.25 ppm. The multiplet at 2.25 ppm, which arises from the H4 and H4′ spins resonating closely to each other, is larger than other 2HG multplets. Detection of this 2.25 ppm multiplet is however complicated due to spectral overlap with the adjacent resonances of glutamate (Glu), glutamine (Gln) and GABA (8). Direct detection of the H3 multiplet at 1.9 ppm is challenging due to its proximity to the N-acetylaspartate (NAA) resonance at 2.01 ppm. Finally, the H2 multiplet at 4.02 ppm is partially overlapped with creatine (Cr) (3.92 ppm), phosphocreatine (3.94 ppm), myo-inositol (mI) (4.06 ppm), lactate (Lac) (4.1 ppm), and free choline (4.05 ppm). Several *in-vivo* ^{1}H MRS studies of 2HG, all at 3T, have been reported recently. The MRS methods used include PRESS (point-resolved spectroscopy) (9,10), J difference editing of the 4.02 ppm resonance (10,11), and 2D shift correlation MRS (11). Given that PRESS and STEAM (stimulated-echo acquisition mode) sequences are readily available for MRS on most clinical scanners and that the data analysis is relatively straightforward using vendor-supplied or commercially available spectral fitting algorithms, measurement of 2HG by these methods could become a valuable clinical application.

While data acquisition with short TE permits the metabolite signals to be acquired with minimal T_2 signal loss, long-TE approaches allow for the acquisition of metabolite signals with attenuated macromolecule baselines and provide the opportunity to optimize the TE to improve differentiation between the overlapped J-coupled resonances. Since the signals from J-coupled spins are influenced by radio-frequency (RF) pulses (12–14) in PRESS, which is widely used for brain MRS at 3T, metabolite estimation may depend on how the basis spectra are generated for spectral fitting. *In-vivo* experimental studies for comparison of short- and long-TE MRS performance, in particular including the oncometabolite 2HG in patient populations, have not been reported to date. Here, we present a comparative study of a short-TE (35 ms) and a previously-reported long-TE (97 ms) (10) PRESS methods for measurement of 2HG in gliomas at 3T. Given that basis spectra calculated using idealized

RF pulses are used for spectral fitting in many studies, we have investigated the utility of both echo times using basis functions generated from 3D volume localized numerical simulations and from non-volume localized simulations in phantoms. The performance of the short and long TE PRESS methods is evaluated using *in-vivo* data from normal brain and tumors.

MATERIALS AND METHODS

The PRESS sequences for studying the performance of short- and long-TE MRS for 2HG detection at 3T used identically shaped 90° excitation RF pulses (9.8 ms; bandwidth = 4.22 kHz at half amplitude), whose amplitude and frequency modulations are shown in a prior study (fremex05) (15). The 180° pulses were different between the sequences. The short-TE PRESS had a 6.9 ms long amplitude-modulated 180° RF pulse, whose envelope is shown in Fig. 1b. The bandwidth of this 180° pulse was 1.26 kHz at an RF field intensity (B_1) of 13.5 μT. Given that echo times between 30 and 40 ms were used in many prior studies (16) and that a TE of 40 ms was advantageous over TE = 30 ms for Glu detection in a prior study (17), the echo time of the short-TE PRESS was set to 35 ms, with the first and second subecho times, TE_1 and TE_2, being 21 and 14 ms, respectively. The long-TE PRESS sequence included a 13.2 ms amplitude-modulated 180° pulse (Fig. 1d), whose bandwidth was also 1.26 kHz at B_1 = 13.5 μT. The subecho times of this PRESS sequence were set to (TE_1, TE_2) = (32, 65) ms, which was obtained with numerical simulations for detecting the 2HG 2.25 ppm signal previously (10). The 13.2 ms 180° pulse was not used for the short-TE PRESS because it did not allow a TE of 35 ms to be achieved using the chosen gradient pulses (*e.g.*, 2.5 ms for each spoiler). For data analysis, two sets of basis spectra were created with numerical density-matrix simulations for each PRESS sequence (TE = 35 and 97 ms); a non-volume localized basis (NLB) and a 3D volume-localized basis (VLB). The NLB set was generated using instantaneous (1 ns) RF pulses for 90° and 180° rotations without slice-selective gradient pulses (Fig. 1a,c). The simulation for VLB spectra included the slice-selective RF and gradient pulses by means of the product-operator transformation-matrix algorithm, as described in the Supplementary Information of a prior paper (10,13). A transformation matrix, which represents the time evolution of the product operators during an RF pulse, was created for each slice-selective RF pulse, and used to obtain the density operator at the end of the PRESS sequence. The simulation for a transformation matrix was conducted using a spatial resolution of 1% (*i.e.*, 0.01 = sample length/number of pixels/slice thickness) with slice thicknesses being 50% of the sample dimension along each of the three directions. The RF carrier frequency was set to 2.7 ppm in the simulations.

MR data were acquired using a whole-body 3T scanner with actively-shielded gradient coils (Philips Medical Systems, Best, The Netherlands). A body coil was used for RF transmission and an 8-channel phased-array head coil was used for signal reception. Phantom experiments were conducted with the PRESS TE = 35 and 97 ms sequences and with the STEAM (TE, TM) = (13, 19) ms sequence on two spherical phantoms (inner diameter = 6 cm; pH = 7.2). One phantom contained 2HG (13 mM) and glycine (Gly) (20 mM), and the other one contained 2HG (4 mM), Glu (5 mM), Gln (5 mM), GABA (1 mM), Cr (5.5 mM) and NAA (5.5 mM). Spectra were obtained from a 2×2×2 cm^3 voxel, using a TR of 15 s (> $5T_1$).

In vivo scans using the PRESS sequences were carried out on 7 healthy volunteers (age median 31; range 26 – 49) and on 22 subjects with IDH-mutated gliomas (median age 38, range 23 – 57; 18 IDH1 mutated and 4 IDH2 mutated; 14 oligodendrogliomas, 6 astrocytomas, and 2 secondary glioblastomas). As for patient overlap with our prior study (10), four patients of the study were scanned at later time points (> 1 year) for the present study using both TE = 35 and 97 ms PRESS sequences. The protocol was approved by the

Institutional Review Board of the University of Texas Southwestern Medical Center. Written informed consent was obtained prior to the scans. For *in vivo* scans of healthy volunteers, MRS data were acquired from 2×2×2 cm^3 voxels positioned in the medial occipital lobes (relatively less susceptible to subject motion artifacts), with the number of signal averages (NSA) set to 128. For the tumor subjects, T_2-weighted fluid-attenuated inversion recovery (T_2w FLAIR) images were acquired to identify tumor mass. Spectra were acquired from 2×2×2 cm^3 voxels positioned at the center of the tumor masses with NSA = 128, except for two cases in which the MRS scans were conducted on 1.5×1.5×1.5 cm^3 voxels with NSA = 512. First and second-order shimming was carried out, using FASTMAP (18) on a 5×5×5 cm^3 volume that included the MRS voxel. Data acquisition parameters included: TR = 2.0 s, sweep width = 2500 Hz, number of sampling points = 2048, and TE = 35 and 97 ms. Spectra were acquired in multiple blocks, each with 4 averages. A 64-step phase cycling scheme was employed (four steps for each RF pulse of PRESS). A vendor-supplied four-pulse variable-flip-angle subsequence was used for water suppression. To minimize the overall metabolite resonance voxel shifts from the planned voxel, the carrier frequencies of the PRESS RF pulses were set to 2.7 ppm (halfway between 1.3 and 4.1 ppm), for which the slice of the 2HG 2.25 ppm resonance was shifted by 1.4% and 4.6% with respect to the slice thicknesses of the 90° and 180° RF pulses, respectively. Following each water-suppressed PRESS acquisition, an unsuppressed PRESS water signal was acquired with 4 averages (TR = 2 s) for eddy current compensation using the same gradient scheme but with the RF carrier frequencies set to the water resonance. In addition, an unsuppressed water signal was acquired from each voxel using STEAM (TE, TM) = (13, 19) ms and TR = 20 s (2 averages) and this short-TE water signal with minimal T_2 relaxation effects was used as a reference for metabolite quantification.

Individual blocks of the multi-block data were processed for correction of eddy current and frequency drift artifacts using an in-house Matlab program (The MathWorks Inc.). Residual eddy current effects were removed using the unsuppressed PRESS water signal (19). The frequency drifts were corrected using a prominent singlet (e.g., Cho at 3.20 ppm or NAA at 2.01 ppm) as a reference. Data were apodized with a 1-Hz exponential function prior to Fourier transformation. LCModel software (20) was used for spectral fitting, using numerically-simulated spectra of 20 metabolites as a basis set. The basis sets included spectra of 2HG, Cr, NAA, GABA, Glu, Gln, mI, Gly, Lac, GSH (glutathione), Ala (alanine), Ace (acetate), Asp (aspartate), Eth (ethanolamine), PE (phosphorylethanolamine), sI (*scyllo*-inositol), Tau (taurine), NAAG (N-acetylaspartylglutamate), Glc (glucose), and Cho (glycerophosphorylcholine + phosphorylcholine + free choline). The spectral fitting was conducted between 0.5 and 4.2 ppm. Cramér-Rao lower bounds (CRLB), returned as percentage standard deviation by LCModel, were used for determining the precision of the metabolite estimates. Metabolite concentrations, C_m, were estimated from LCModel estimates of metabolite signals, S_m, and the short-TE, long-TR STEAM water signals multiplied by 2, S_w, using the equation

$$C_m = C_w (S_m/S_w) exp(\mathrm{TE_{diff}}/T_2)/[1-exp(-\mathrm{TR}/T_1)], \quad [1]$$

where TE_{diff} was the TE difference between the PRESS and STEAM acquisitions, neglecting the errors due to the mismatch between the STEAM and PRESS localized voxel shapes. The signal decay ratio between water and metabolites at TE = 13 ms was ignored. A water concentration C_w of 42.2 M was used for both normal brain and tumors, similarly to a prior study (10). Relaxation effects on metabolite signals were corrected using published metabolite T_2 and T_1 values: T_2 = 150 ms, 230 ms and 280 ms for Cr, Cho and NAA, respectively, and 180 ms for other metabolites; T_1 = 1.2 s for 2HG, Glu, Gln and mI, and 1.5 s for other metabolites (21–23).

RESULTS

Figure 1 shows spectra of 2HG and several metabolites with resonances in the proximity of the 2HG 2.25 ppm resonance, which were numerically-calculated for non-localized and 3D volume-localized double-echo sequences with TE = 35 and 97 ms. To make a direct comparison of the signal strengths, the non-volume localized spectra were scaled by the ratio of the PRESS-prescribed 3D volume to the entire sample volume. Since the slice thickness in each direction was 50% of the entire sample length, this volume ratio was 0.125 (= 0.5×0.5×0.5). The NAA singlets (2.01 ppm) of the spectra simulated for the PRESS sequences using 6.9 and 13.2 ms 180° pulses were 83.6% and 93.5% of the scaled signal from the non-volume localized spectra, respectively. The substantial signal loss of the 6.9 ms 180° RF pulses as compared to the 13.2 ms 180° pulses was primarily due to imperfect refocusing which resulted from the large ripples in the refocusing profile (Fig. 1b). For J-coupled resonances, the signal intensity and pattern also depended on both the refocusing profile and the spectral distance between the coupling partners relative to the RF pulse bandwidth. For TE = 35 ms, the spectral patterns of 2HG, Glu, Gln and GABA at 1.8 – 2.6 ppm were similar between non-localized and volume-localized simulations due to the minimal J evolution during the short TE and the relatively small spectral distances between coupling partners. However, the resonances between 2.9 and 4.1 ppm exhibited different patterns between non-localized and volume-localized spectra, primarily due to the increased chemical shift displacement effects (16). For TE = 97 ms, the spectral discrepancy between non-localized and volume-localized spectra was extensive over the entire range of 1.8 and 4.1 ppm due to the effects of the J evolution during the long echo time. The multiplets of 2HG, Glu, Gln and GABA between 1.8 and 2.2 ppm were decreased in the volume localized spectra. The volume-localized NAA multiplets were also quite different from the non-localized signals.

Figure 2 presents phantom spectra of 2HG obtained with PRESS TE = 35 and 97 ms and STEAM TE = 13 ms, together with 2HG spectra calculated with volume-localized and nonlocalized simulations. The phantom data indicated that, for identically prescribed volumes, the Gly singlets from the TE = 35 ms PRESS and the TE = 13 ms STEAM were 92.8 and 52.6% with respect to the Gly signal from the TE = 97 ms PRESS, which was in good agreement with the simulation results after correcting for the T_2 effects in the phantom solution (Gly $T_2 \approx 1500$ ms). The higher Gly signal at the long-TE PRESS, as compared to the short-TE PRESS, can be explained by the better refocusing performance of the 13.2 ms 180° RF pulse used. Stimulated-echo spectra of 2HG were essentially the same between volume-localized and non-localized simulations because of the effects of the relatively large bandwidth (4.2 kHz) of the slice-selective 90° RF pulse and the minimal J evolution during the short TE, resulting in both simulations reproducing the phantom data closely. For the double-echo case, however, a notable difference was observed between the simulations. While the volume-localized simulations closely reproduced the phantom PRESS spectra in the entire spectral region, the non-localized simulations resulted in large discrepancy of H2, H3 and H3′ multiplets from experiments at both TEs, primarily due to the effects of the relatively small bandwidth of the 180° pulses (1.26 kHz). The H4, H4′, H3 and H3′ multiplets appeared extensively overlapped at TE = 35 ms. At TE = 97 ms, the H3 and H3′ resonances were drastically attenuated, leading to a narrow 2HG signal at 2.25 ppm (H4 and H4′ spins) observable in both the volume-localized phantom and calculated spectra. For the prepared 2HG-to-Gly concentration ratio of 0.65 in the phantom, the 2HG 2.25 ppm multiplet amplitude was 13.1% of the Gly signal in the PRESS 97 ms spectrum. The 2HG 2.25 ppm signal yield of the PRESS 97 ms with respect to 90°-acquisition was estimated to be 63%, ignoring T_2 relaxation effects.

Figure 3 displays *in-vitro* spectra from a composite phantom solution and the LCModel analysis results. The spectra obtained with the TE = 35 and 97 ms PRESS sequences were processed using basis sets generated by non-localized and volume-localized double-echo simulations (NLB and VLB, respectively). For the PRESS TE = 35 ms phantom data, the LCModel analysis with NLB resulted in large residuals in the entire spectral region, giving estimates of 2HG, Glu, Gln and GABA of 2.7, 5.3, 4.7 and 0.4 mM, with CRLBs of 7, 3, 4 and 19%, respectively (Fig. 3a). These estimates were quite different from the prepared concentrations (4, 5, 5 and 1 mM, respectively). Using VLB, the reproduction of the phantom spectrum was improved notably, as indicated by reduced residuals and CRLBs (Fig. 3b). The estimates of the compounds were in good agreement with the prepared concentrations. For PRESS TE = 97 ms, the phantom spectrum was not well reproduced by NLB (Fig. 3c), as indicated by the large residuals similar to those found in short-TE PRESS. The residuals were substantially decreased when VLB was used for fitting (Fig. 3d), giving small CRLBs and reproducing the prepared concentrations following the correction for T_2 effects on the 2HG, Glu, Gln and GABA signals using the 2HG T_2 value (700 ms) of the phantom of Fig. 2. The discrepancy of the concentration estimates from the prepared concentrations was the largest in PRESS 97 ms NLB, in which underestimation of the concentrations occurred because larger signals resulted from the non-localized simulations compared to the volume-localized simulations, as shown in Fig. 1.

Given the large discrepancy between the non-volume localized simulations and phantom experiments, *in vivo* brain data, obtained with PRESS TE = 35 and 97 ms, were analyzed with volume localized basis sets only. Representative *in-vivo* spectra from a healthy volunteer and a subject with IDH-mutated glioma are presented in Fig. 4. In the normal subject, 2HG was undetected at both TEs. The concentrations of Glu, Gln and GABA were estimated to be about the same using TE = 35 and 97 ms following the correction of T_2 effects, with CRLBs all less than 20%. The CRLBs of the metabolites were lower at TE = 97 ms than at TE = 35 ms, which indicates improved precision by the long TE method. For the tumor subject, the PRESS 35 and 97 ms spectra both showed spectral patterns at 2.2 – 2.5 ppm that are indicative of elevated 2HG and decreased Glu. 2HG was measurable by both TEs, but the concentration estimates were somewhat different between the TEs. The 2HG CRLB was smaller at TE = 97 ms than at TE = 35 ms (6% *vs.* 9%), indicating improved 2HG detectability by the long TE. CRLB reduction by the long TE was also the case for Glu and Gln. The Glu and Gln levels were measured to be 2 –3 mM in the tumor, while GABA was not detected reliably.

Table 1 presents concentration estimates and CRLBs of 2HG, Glu, Gln and GABA in the 7 healthy volunteers and 22 subjects with IDH mutated gliomas, obtained from PRESS TE = 35 and 97 ms data analyzed with volume localized basis sets. For the 7 healthy subjects, the 2HG estimate was negligible or essentially zero in most cases, with CRLB ≥20% in all cases. For 2×2×2 cm^3 voxels positioned in the medial occipital lobes of normal brain, PRESS TE = 35 and 97 ms gave similar concentration estimates of Glu, Gln and GABA following correction of the T_2 effects (approximately 9, 2 and 1 mM, respectively). However, the CRLBs of the metabolites were different between the methods. While the long TE method gave CRLBs of Glu, Gln and GABA at less than 20% in most cases, CRLB < 20% occurred only in a subset of subjects at short TE (*i.e.*, 7, 6, and 3 cases for Glu, Gln and GABA, respectively). The mean CRLBs of Glu, Gln and GABA were smaller at TE = 97 ms than at TE = 35 ms. Tumor data showed greater difference in CRLB between the methods. Of the 22 gliomas with IDH mutations, 2HG CRLB < 20% was observed in all 22 subjects by the PRESS 97 ms and in 17 subjects by the PRESS 35 ms. For these cases, the mean 2HG CRLB was lower at TE = 97 ms than at TE = 35 ms (8.5% *vs.* 11.6%), showing overall higher 2HG estimates from the long TE data. As a result, the mean standard deviation of 2HG estimates (= mean C_m× mean CRLB/100) was slightly smaller in the TE = 35 method

(0.28 mM = 2.4×11.6/100) than in the TE = 97 ms method (0.30 mM = 3.5×8.5/100). For comparison, when including the data from the 5 subjects in the calculation, in whom the TE = 35 ms failed to detect 2HG with CRLB < 20%, the mean 2HG concentration and CRLB of the TE = 35 ms method were calculated to be 2.1 mM and 62.5%, giving a much larger mean 2HG standard deviation (1.3 mM) compared to the 97 ms method. The CRLBs of Glu and Gln by the long TE were smaller than 20% in all subjects, while the short TE data showed CRLB < 20% for Glu and Gln in 20 and 18 subjects, respectively. While Gln levels were observed to be greater or similar in tumors compared to normal brain, Glu was decreased in all tumors (< 5 mM), resulting in CRLB much larger than in normal brain in both methods. The GABA CRLB was less than 20% only in a small number of cases.

DISCUSSION

The current paper reports a comparative study of TE = 35 and 97 ms PRESS sequences, focusing on 2HG detection in IDH-mutated gliomas. Although use of identical 180° pulses would be most ideal for comparison between echo times, given that the 6.9 ms 180° pulse of the PRESS 35 ms sequence was used in many prior short-TE studies (15,24) and the refocusing bandwidths of the 180° RF pulses are identical, the two PRESS sequences investigated in this study are reasonable choices for short- and long-TE PRESS protocols for comparing 2HG detectability. The PRESS 97 ms sequence has several strengths compared to the PRESS 35 ms sequence. With the refocusing profile of the 13.2 ms 180° RF pulse with small ripples and narrow transition widths compared to the 6.9 ms 180° pulse (transition width 12% *vs.* 19% relative to the bandwidth at half amplitude), the PRESS 97 ms sequence permits more favorable voxel localization. Moreover, the 97 ms echo time produces a well-defined narrow 2HG signal at 2.25 ppm, thereby leading to improved differentiation between 2HG and the adjacent Glu, Gln and GABA signals. We consider the use of hard-pulse generated non-localized basis sets for spectral fitting to be suboptimal for 2HG detection at both short and long TEs since the simulated spectra are notably different from spectra produced in phantom experiments. This difference in 2HG signals is attributable to the substantial difference between the time evolution of coherences during a hard-pulse dual-echo sequence and during a PRESS sequence with finite-bandwidth RF pulses for volume localization (12–14). Although the 2HG H4 and H4′ multiplet pattern from non-localized simulations appears similar to the spectral pattern in phantom data, the H3, H3′ and H2 multiplets differ substantially between the simplified simulation and experiment, thereby leading to suboptimal fits of 2HG and other J-coupled metabolite signals (see Fig. 3). Together, use of volume localized basis spectra may be essential for evaluating the metabolite signals in PRESS data properly, specifically for assessing the signals of 2HG that has strongly-coupled spins as well as weakly-coupled resonances separated by large spectral distances.

Short and long TE MRS methods have pros and cons in metabolite quantification *in vivo*. Measurements with short TE, under a fairly long TR, may permit the acquisition of the full metabolite signal and thus would be preferable for accurate quantification of 2HG. However, detectability is reduced by the presence of large baseline macromolecule signals and spectral overlap of the broad 2HG multiplets with neighboring resonances, resulting in failure of 2HG detection with acceptable precision in 5 of the 22 patients. Spectral fitting of PRESS TE = 97 ms data is markedly simplified due to the effects of attenuated macromolecule signals (see Fig. 4), with an additional advantage that discrimination between the J-coupled resonances at 2.2 – 2.5 ppm is improved due to the narrowing of the multiplets, thereby allowing precise estimation of the signal strengths. High flexibility in choosing RF pulse type on the prolonged subecho times is another benefit, which was utilized in the current study. Although the accuracy of 2HG estimates by the PRESS 97 ms is limited by the T_2 relaxation effects, CRLB reduction by the method may increase greatly

the clinical applicability of this first ever imaging biomarker that appears to be specific for IDH-mutated gliomas and therefore may have important implications for use in management of patients with brain tumors. Given that a CRLB is a measure of the probability of presence of 2HG on MRS (*e.g.*, 95% confidence interval ≈ 1.96×CRLB), low CRLB is important for the development of 2HG clinical application. The reduced 2HG CRLB from PRESS 97 could also provide the level of precision necessary to develop 2HG evaluation for use as a surrogate marker for tumor growth or response to treatment. This is of particular importance now as the first inhibitor of IDH1 is entering early phase clinical trials (25) and precise 2HG measurement by MRS could provide the first non-invasive imaging biomarker for clinical trials.

In most of the tumor subjects enrolled in this study, Glu was substantially decreased and Gln was somewhat increased compared to normal brain, as shown in Table 1. A similar phenomenon was observed through metabolite measurements in an orthotopic model of human gliomas grown in the mouse brain, where the tumors had high Gln to Glu ratios compared to the normal brain (26). Neither Glu or Gln concentration was correlated with 2HG concentration, as indicated by small coefficients of determination (R^2) (< 0.1) in a linear regression of Glu or Gln estimates *vs.* 2HG estimates (data not shown). This suggests that the alterations in Glu and Gln levels are independent of the production of 2HG in IDH-mutated gliomas. This conclusion differs from the result of a recent *ex vivo* MRS study (27), which reported a significant linear correlation between Glu and 2HG levels. A significant correlation was not observed between Glu and Gln levels in our data. While GABA levels were normal (~1 mM) in some patients as measured by PRESS 97 ms, GABA was not detectable in many tumor subjects.

The current study used short-TE STEAM water signal (TE = 13 ms) as a reference for metabolite quantification, ignoring the effects of T_2 relaxation during the STEAM TE on the water and metabolite signals. While the uncertainties in metabolite estimates can be theoretically minimized by means of external reference signals (28–30), brain water signals may provide a reasonable internal reference for quantifying metabolic alterations in tumors (31). As opposed to the single-TE water acquisition method, which was chosen for minimizing the scan time for reference signal acquisition in this study, use of zero-TE water signal from multi-TE experiments would be ideal since water T_2 relaxation may be multi-exponential due to the tissue heterogeneity within the voxel (gray and white matter, cerebrospinal fluids, and tumor to normal brain fractions). In addition, since a constant water concentration of 42.2 M was used, error will be introduced in the metabolite estimation when the water concentration in the tumor is different from the assumed value.

CONCLUSION

Compared to standard short-TE PRESS methods at 3T, the 2HG-optimized TE = 97 ms PRESS sequence provides enhanced selectivity and specificity for 2HG as well as for Glu, Gln and GABA. This improved capability of estimating the J-coupled spin metabolites using this sequence is gained by means of spectral analysis using basis functions generated from the specific sequence components used for data acquisition. 2HG measurement *in vivo* is anticipated to become an important clinical tool for noninvasive diagnosis of gliomas. Furthermore, it may become possible to use 2HG as a dynamic biomarker of disease in which precise measurement of its concentration will be important in evaluating tumor progression, response to treatment, or recurrence. Given the proximity of the 2HG signals to other metabolite signals, the ability to alleviate the spectral complexities in the 2HG measurement will be important for increasing the clinical potential of this recently discovered oncometabolite.

Acknowledgments

This work was supported by US National Institutes of Health grants, R21CA159128, R01CA154843, and R01CA157996, and by Cancer Prevention Research Institute of Texas grants RP101243-P04 and RP130427.

Abbreviations

2HG	2-hydroxyglutarate
Ace	acetate
Ala	alanine
Asp	aspartate
Cho	glycerophosphorylcholine + phosphorylcholine + free choline
CRLB	Cramér-Rao lower bound
Cr	creatine
Eth	ethanolamine
FASTMAP	fast automatic shimming technique by mapping along projections
GABA	γ-aminobutyric acid
Glc	glucose
Gln	glutamine
Glu	glutamate
Gly	glycine
GSH	glutathione
IDH	isocitrate dehydrogenase
Lac	lactate
mI	myo-inositol
NAA	N-acetylasparate
NAAG	N-acetlyaspartylglutamate
$NADP^+$	nicotinamide adenine dinucleotide phosphate
NLB	non-volume localized basis
NSA	number of signal averages
PE	phosphorylethanolamine
PRESS	point-resolved spectroscopy
RF	radio-frequency
sI	*scyllo*-inositol
STEAM	stimulated-echo acquisition mode
T_2w FLAIR	T_2-weighted fluid-attenuated inversion recovery
Tau	taurine
VLB	volume-localized basis

References

1. Parsons DW, Jones S, Zhang X, Lin JC, Leary RJ, Angenendt P, Mankoo P, Carter H, Siu IM, Gallia GL, Olivi A, McLendon R, Rasheed BA, Keir S, Nikolskaya T, Nikolsky Y, Busam DA, Tekleab H, Diaz LA Jr, Hartigan J, Smith DR, Strausberg RL, Marie SK, Shinjo SM, Yan H, Riggins GJ, Bigner DD, Karchin R, Papadopoulos N, Parmigiani G, Vogelstein B, Velculescu VE, Kinzler KW. An integrated genomic analysis of human glioblastoma multiforme. Science. 2008; 321:1807–1812. [PubMed: 18772396]
2. Yan H, Parsons DW, Jin G, McLendon R, Rasheed BA, Yuan W, Kos I, Batinic-Haberle I, Jones S, Riggins GJ, Friedman H, Friedman A, Reardon D, Herndon J, Kinzler KW, Velculescu VE, Vogelstein B, Bigner DD. IDH1 and IDH2 mutations in gliomas. N Engl J Med. 2009; 360:765–773. [PubMed: 19228619]
3. Dang L, White DW, Gross S, Bennett BD, Bittinger MA, Driggers EM, Fantin VR, Jang HG, Jin S, Keenan MC, Marks KM, Prins RM, Ward PS, Yen KE, Liau LM, Rabinowitz JD, Cantley LC, Thompson CB, Vander Heiden MG, Su SM. Cancer-associated IDH1 mutations produce 2-hydroxyglutarate. Nature. 2009; 462:739–744. [PubMed: 19935646]
4. Figueroa ME, Abdel-Wahab O, Lu C, Ward PS, Patel J, Shih A, Li Y, Bhagwat N, Vasanthakumar A, Fernandez HF, Tallman MS, Sun Z, Wolniak K, Peeters JK, Liu W, Choe SE, Fantin VR, Paietta E, Lowenberg B, Licht JD, Godley LA, Delwel R, Valk PJ, Thompson CB, Levine RL, Melnick A. Leukemic IDH1 and IDH2 mutations result in a hypermethylation phenotype, disrupt TET2 function, and impair hematopoietic differentiation. Cancer Cell. 2010; 18:553–567. [PubMed: 21130701]
5. Ward PS, Patel J, Wise DR, Abdel-Wahab O, Bennett BD, Coller HA, Cross JR, Fantin VR, Hedvat CV, Perl AE, Rabinowitz JD, Carroll M, Su SM, Sharp KA, Levine RL, Thompson CB. The common feature of leukemia-associated IDH1 and IDH2 mutations is a neomorphic enzyme activity converting alpha-ketoglutarate to 2-hydroxyglutarate. Cancer Cell. 2010; 17:225–234. [PubMed: 20171147]
6. Lu C, Ward PS, Kapoor GS, Rohle D, Turcan S, Abdel-Wahab O, Edwards CR, Khanin R, Figueroa ME, Melnick A, Wellen KE, O'Rourke DM, Berger SL, Chan TA, Levine RL, Mellinghoff IK, Thompson CB. IDH mutation impairs histone demethylation and results in a block to cell differentiation. Nature. 2012; 483:474–478. [PubMed: 22343901]
7. Bal D, Gryff-Keller A. 1H and 13C NMR study of 2-hydroxyglutaric acid and its lactone. Magn Reson Chem. 2002; 40:533–536.
8. Govindaraju V, Young K, Maudsley AA. Proton NMR chemical shifts and coupling constants for brain metabolites. NMR Biomed. 2000; 13:129–153. [PubMed: 10861994]
9. Pope WB, Prins RM, Albert Thomas M, Nagarajan R, Yen KE, Bittinger MA, Salamon N, Chou AP, Yong WH, Soto H, Wilson N, Driggers E, Jang HG, Su SM, Schenkein DP, Lai A, Cloughesy TF, Kornblum HI, Wu H, Fantin VR, Liau LM. Non-invasive detection of 2-hydroxyglutarate and other metabolites in IDH1 mutant glioma patients using magnetic resonance spectroscopy. J Neurooncol. 2012; 107:197–205. [PubMed: 22015945]
10. Choi C, Ganji SK, Deberardinis RJ, Hatanpaa KJ, Rakheja D, Kovacs Z, Yang XL, Mashimo T, Raisanen JM, Marin-Valencia I, Pascual JM, Madden CJ, Mickey BE, Malloy CR, Bachoo RM, Maher EA. 2-hydroxyglutarate detection by magnetic resonance spectroscopy in IDH-mutated patients with gliomas. Nat Med. 2012; 18:624–629. [PubMed: 22281806]
11. Andronesi OC, Kim GS, Gerstner E, Batchelor T, Tzika AA, Fantin VR, Vander Heiden MG, Sorensen AG. Detection of 2-hydroxyglutarate in IDH-mutated glioma patients by in vivo spectral-editing and 2D correlation magnetic resonance spectroscopy. Sci Transl Med. 2012; 4:116ra114.
12. Slotboom J, Mehlkope AF, Bovee WMMJ. The effects of frequency-selective RF pulses on J-coupled spin-1/2 systems. J Magn Reson A. 1994; 108:38–50.
13. Thompson RB, Allen PS. Sources of variability in the response of coupled spins to the PRESS sequence and their potential impact on metabolite quantification. Magn Reson Med. 1999; 41:1162–1169. [PubMed: 10371448]
14. Kaiser LG, Young K, Matson GB. Numerical simulations of localized high field ^{1}H MR spectroscopy. J Magn Reson. 2008; 195:67–75. [PubMed: 18789736]

15. Henning A, Fuchs A, Murdoch JB, Boesiger P. Slice-selective FID acquisition, localized by outer volume suppression (FIDLOVS) for ^{1}H-MRSI of the human brain at 7 T with minimal signal loss. NMR Biomed. 2009; 22:683–696. [PubMed: 19259944]
16. Barker, PB.; Bizzi, A.; De Stefano, N.; Gullapalli, RP.; Lin, DDM. Clinical MR Spectroscopy: Techniques and Applications. Cambridge: Cambridge University Press; 2010.
17. Mullins PG, Chen H, Xu J, Caprihan A, Gasparovic C. Comparative reliability of proton spectroscopy techniques designed to improve detection of J-coupled metabolites. Magn Reson Med. 2008; 60:964–969. [PubMed: 18816817]
18. Gruetter R. Automatic, localized in vivo adjustment of all first- and second-order shim coils. Magn Reson Med. 1993; 29:804–811. [PubMed: 8350724]
19. Klose U. In vivo proton spectroscopy in presence of eddy currents. Magn Reson Med. 1990; 14:26–30. [PubMed: 2161984]
20. Provencher SW. Estimation of metabolite concentrations from localized in vivo proton NMR spectra. Magn Reson Med. 1993; 30:672–679. [PubMed: 8139448]
21. Mlynarik V, Gruber S, Moser E. Proton T_1 and T_2 relaxation times of human brain metabolites at 3 Tesla. NMR Biomed. 2001; 14:325–331. [PubMed: 11477653]
22. Traber F, Block W, Lamerichs R, Gieseke J, Schild HH. ^{1}H metabolite relaxation times at 3. 0 tesla: Measurements of T_1 and T_2 values in normal brain and determination of regional differences in transverse relaxation. J Magn Reson Imaging. 2004; 19:537–545. [PubMed: 15112302]
23. Ganji SK, Banerjee A, Patel AM, Zhao YD, Dimitrov IE, Browning JD, Brown ES, Maher EA, Choi C. T_2 measurement of J-coupled metabolites in the human brain at 3T. NMR Biomed. 2012; 25:523–529. [PubMed: 21845738]
24. Edden RA, Barker PB. If J doesn't evolve, it won't J-resolve: J-PRESS with bandwidth-limited refocusing pulses. Magn Reson Med. 2011; 65:1509–1514. [PubMed: 21590799]
25. Popovici-Muller J, Saunders JO, Salituro FG, Travins JM, Yan S, Zhao F, Gross S, Dang L, Yen KE, Yang H, Straley KS, Jin S, Kunii K, Fantin VR, Zhang S, Pan Q, Shi D, Biller SA, Su SM. Discovery of the First Potent Inhibitors of Mutant IDH1 That Lower Tumor 2-HG *in Vivo*. ACS Med Chem Lett. 2012; 3:850–855.
26. Marin-Valencia I, Yang C, Mashimo T, Cho S, Baek H, Yang XL, Rajagopalan KN, Maddie M, Vemireddy V, Zhao Z, Cai L, Good L, Tu BP, Hatanpaa KJ, Mickey BE, Mates JM, Pascual JM, Maher EA, Malloy CR, Deberardinis RJ, Bachoo RM. Analysis of tumor metabolism reveals mitochondrial glucose oxidation in genetically diverse human glioblastomas in the mouse brain in vivo. Cell Metab. 2012; 15:827–837. [PubMed: 22682223]
27. Elkhaled A, Jalbert LE, Phillips JJ, Yoshihara HA, Parvataneni R, Srinivasan R, Bourne G, Berger MS, Chang SM, Cha S, Nelson SJ. Magnetic resonance of 2-hydroxyglutarate in IDH1-mutated low-grade gliomas. Sci Transl Med. 2012; 4:116ra115.
28. Kreis R. Quantitative localized 1H MR spectroscopy for clinical use. Prog Nuc Magn Reson Spec. 1997; 31:155–195.
29. Keevil SF, Barbiroli B, Brooks JC, Cady EB, Canese R, Carlier P, Collins DJ, Gilligan P, Gobbi G, Hennig J, Kugel H, Leach MO, Metzler D, Mlynarik V, Moser E, Newbold MC, Payne GS, Ring P, Roberts JN, Rowland IJ, Thiel T, Tkac I, Topp S, Wittsack HJ, Wylezinska M, Zaniol P, Henriksen O, Podo F. Absolute metabolite quantification by in vivo NMR spectroscopy: II. A multicentre trial of protocols for in vivo localised proton studies of human brain. Magn Reson Imaging. 1998; 16:1093–1106. [PubMed: 9839993]
30. Martinez-Bisbal MC, Monleon D, Assemat O, Piotto M, Piquer J, Llacer JL, Celda B. Determination of metabolite concentrations in human brain tumour biopsy samples using HR-MAS and ERETIC measurements. NMR Biomed. 2009; 22:199–206. [PubMed: 18833546]
31. Tong Z, Yamaki T, Harada K, Houkin K. In vivo quantification of the metabolites in normal brain and brain tumors by proton MR spectroscopy using water as an internal standard. Magn Reson Imaging. 2004; 22:1017–1024. [PubMed: 15288143]

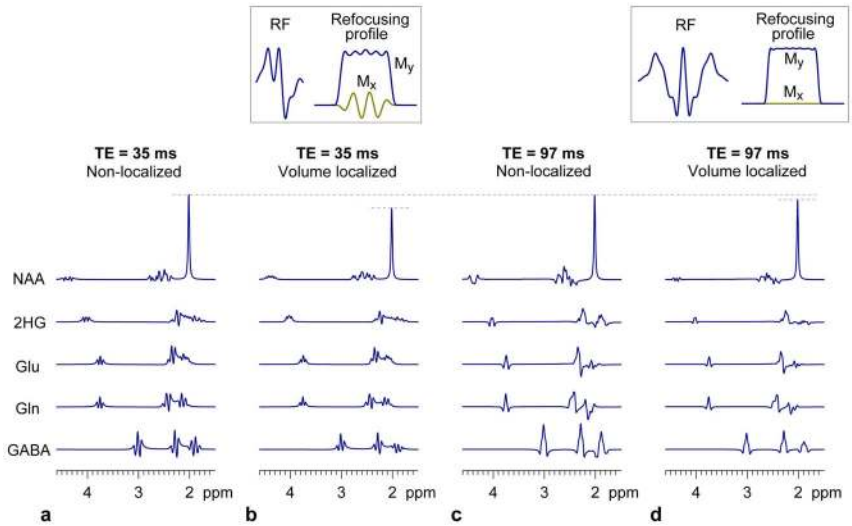

FIG. 1.

Numerically-calculated spectra of NAA, 2HG, Glu, Gln and GABA, following non-volume selective and 3D volume-selective double-echo sequences (90° - $TE_1/2$ - 180° - $TE_1/2$ - $TE_2/2$ - 180° - $TE_2/2$) at (TE_1, TE_2) = (21, 14) and (32, 65) ms, are shown together with the RF envelopes and calculated refocusing profiles of the slice-selective 180° pulses. The 180° pulses of the volume-localized spectra at TE = 35 and 97 ms were amplitude-modulated 6.9 and 13.2 ms pulses, respectively, both with refocusing bandwidth of 1.26 kHz at B_1 = 13.5 μT. Nonlocalized spectra were calculated using instantaneous RF pulses (1 ns long), and then scaled according to the ratio of the localized volume to the entire volume (*i.e.*, 0.5×0.5×0.5 = 0.125). The refocusing profile was numerically calculated from M_y prior to the 180° pulse using a 2-step phase cycling (0 and π/2). Spectra were broadened to singlet linewidth (FWHM) of 4 Hz.

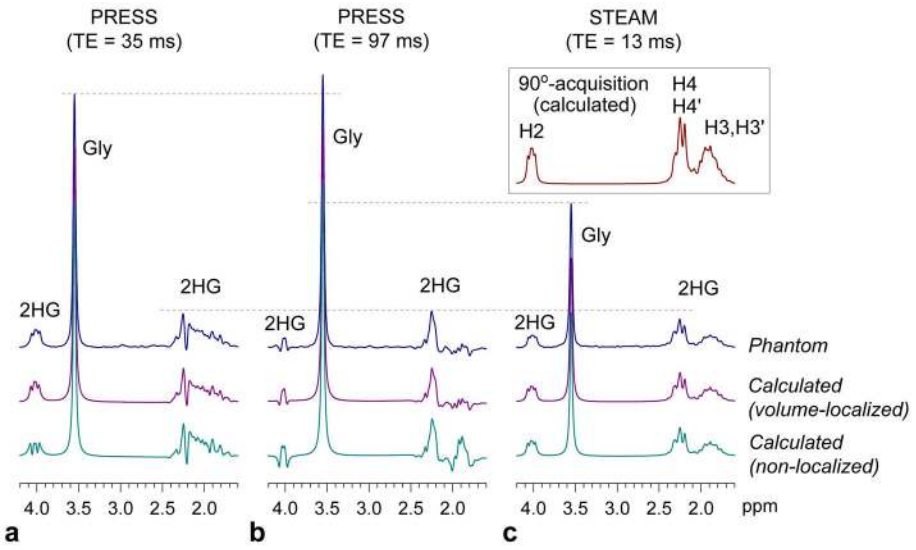

FIG. 2.

Phantom spectra of 2HG (13 mM) and Gly (20 mM), obtained with PRESS TE = 35 and 97 ms and STEAM (TE, TM) = (13, 19) ms, are shown together with non-volume localized and 3D volume localized calculated spectra. The calculated signals were adjusted using phantom T_2's of Gly (1400 ms) and 2HG (700 ms). The inset shows a calculated 90°-acquired 2HG spectrum, which was scaled to reflect the prescribed voxel volume of the PRESS and STEAM sequences. Spectra were broadened to singlet linewidth of 4 Hz.

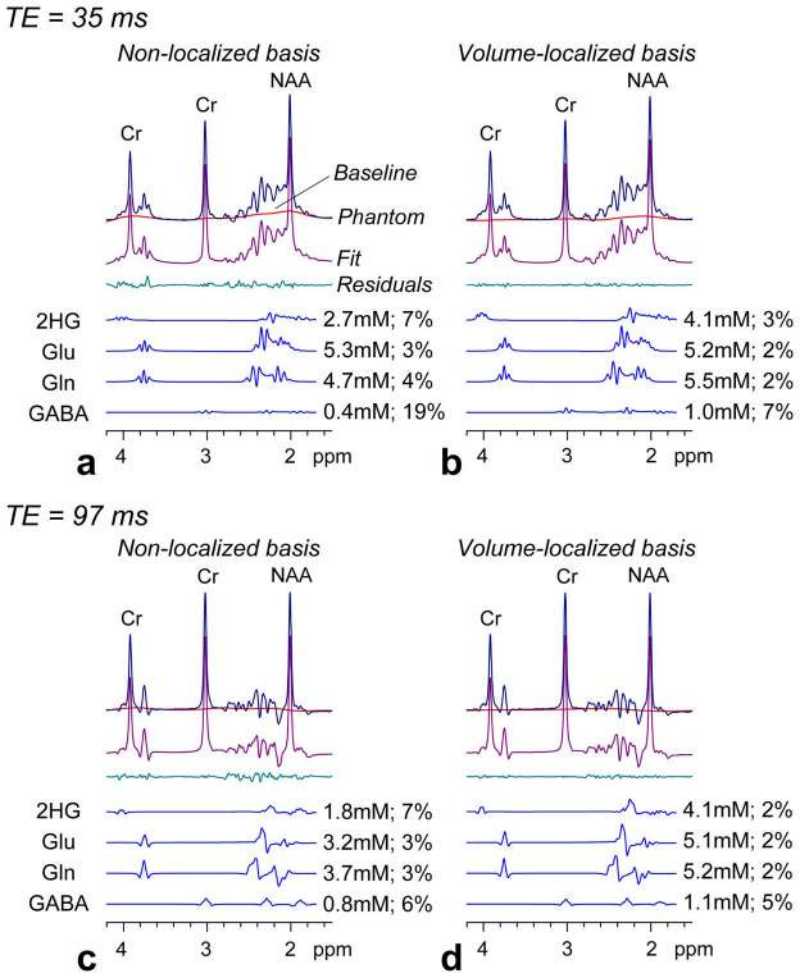

FIG. 3.

Spectra from a composite phantom, obtained with PRESS TE = 35 and 97 ms, are shown together with LCModel fits, residuals and baseline. The individual spectra of 2HG, Glu, Gln, and GABA, generated according to the LCModel estimates are presented together with the estimated concentrations and CRLBs. LCModel analysis was undertaken, for both TEs, using non-volume localized and volume-localized basis sets. The prepared concentrations in the phantom solution were 4, 5, 5, 1, 5.5, and 5.5 mM for 2HG, Glu, Gln, GABA, Cr, and NAA, respectively. The singlet linewidth is 4 Hz in the spectra.

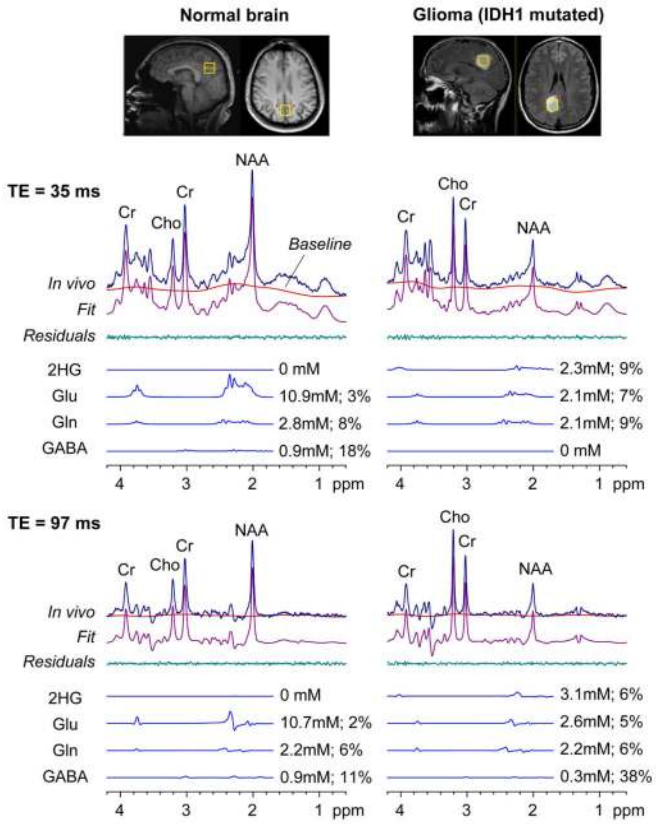

FIG. 4.

In vivo brain spectra from a healthy volunteer and a patient with an IDH-mutated glioma, obtained with PRESS TE = 35 and 97 ms at 3T, are shown with voxel positioning (voxel size 2×2×2 cm^3) on T_2w-FLAIR images. LCModel fitting results, obtained with volume-localized basis sets, are presented in a similar fashion to Fig. 3. Data were acquired with TR = 2 s and 128 averages.

Table 1

Mean concentrations (C_m) and CRLBs of 2HG, Glu, Gln, and GABA in 7 healthy subjects (medial occipital) and 22 patients with IDH-mutated gliomas, obtained from PRESS TE = 35 and 97 ms spectra, are presented in mean ± standard deviation for the cases with CRLB < 20%, indicated by N. The numbers in brackets are the minimum and maximum CRLBs for the data rejected (CRLB ≥20%). Spectra were analyzed, with LCModel, using volume-localized basis sets.

	Healthy volunteers (N_{total} = 7)						IDH-mutated gliomas (N_{total} = 22)					
	TE = 35 ms			TE = 97 ms			TE = 35ms			TE = 97 ms		
	N	C_m (mM)	CRLB (%)	N	C_m (mM)	CRLB (%)	N	C_m (mM)	CRLB (%)	N	C_m (mM)	CRLB (%)
2HG	0	-	- (20, 999)	0	-	- (62, 999)	17	2.4±1.1	11.6±4.0 (24, 999)	22	3.5±1.6	8.5±3.4 (NA)
Glu	7	8.4±1.5	3.3±0.8 (NA)	7	9.3±0.9	2.7±0.8 (NA)	20	2.3±0.7	10.2±3.6 (20, 21)	22	2.9±0.9	7.1±2.4 (NA)
Gln	6	1.8±0.6	11.2±3.3 (74)	7	1.9±0.2	7.1±0.9 (NA)	18	2.5±1.3	10.2±3.4 (22, 35)	22	3.1±1.2	6.4±2.8 (NA)
GABA	3	1.1±0.2	14.0±4.4 (21, 999)	6	0.9±0.1	11.7±2.9 (28)	2	0.9±0.2	15.5±0.7 (22, 999)	7	1.0±0.2	13.9±3.0 (21, 999)